Magnetic Resonance Velocity Imaging Using a Fast Spiral Phase Contrast Sequence

G. Bruce Pike, Craig H. Meyer, Thomas J. Brosnan, Norbert J. Pelc

Time-resolved velocity imaging using the magnetic resonance phase contrast technique can provide clinically important quantitative flow measurements *in vivo* but suffers from long scan times when based on conventional spin-warp sequences. This can be particularly problematic when imaging regions of the abdomen and thorax because of respiratory motion. We present a rapid phase contrast sequence based on an interleaved spiral k-space data acquisition that permits time-resolved, three-direction velocity imaging within a breath-hold. Results of steady and pulsatile flow phantom experiments are presented, which indicate excellent agreement between our technique and through plane flow measurements made with an in-line ultrasound probe. Also shown are results of normal volunteer studies of the carotids, renal arteries, and heart.

Key words: fast magnetic resonance imaging; flow quantitation; velocity imaging; pulse sequences.

INTRODUCTION

The phase contrast velocity imaging technique constitutes a powerful tool for quantitative velocity measurement *in vivo*. The basis of the technique, first described by Hahn (1), is the fact that spins moving within a magnetic field gradient acquire a phase different from stationary spins. Mathematically, for a spatial position function $\mathbf{r}(t)$ and a magnetic field gradient $\mathbf{G}(t)$, the magnetization phase is:

$$\phi(\mathbf{r},t) = \gamma \int_0^t \mathbf{G}(t)\cdot\mathbf{r}(t)dt. \quad [1]$$

For spins moving along the x-axis with a constant velocity v_x, and initial position $r_0 = 0$,

$$\phi(t) = v_x\gamma \int_0^t \mathbf{G}_x(t)tdt. \quad [2]$$

The integral term in this equation is the first moment of the x gradient waveform. Therefore, in general, the phase accrued for a constant velocity spin is

$$\phi = v\gamma M_1, \quad [3]$$

where M_1 is the first moment of the gradient waveform along the direction of v.

The first application of motion induced phase modulation to MRI was developed by Moran (2). In his technique a multiple step flow-induced phase encoding was proposed that is completely analogous to spatial phase encoding in spin-warp imaging. Although this method can in theory image the six dimensional joint position-velocity space, the required imaging time for such an acquisition would be prohibitive. The greatest simplification of this technique is to acquire a single image and to calculate velocities directly from the phase image using Eq. [3]. This approach was first demonstrated by Van Dijk (3) who used the fact that the read-out gradient in a conventional spin-echo sequence has a non-zero first moment and is therefore inherently velocity sensitive. The major limitation of the single phase measurement technique is that phase shifts can also arise from a variety of nonflow-related sources, especially due to B_0 in gradient-echo sequences.

The most common method of velocity imaging using flow-induced phase modulation is to perform two spin-warp data acquisitions in which the first moment of the gradient waveform, along the flow direction of interest, is varied between measurements (4–7). The phase difference between these measurements is then directly proportional to velocity only (ignoring higher order motion terms, eddy currents, and assuming a relatively uniform velocity within a voxel). This technique has come to be known as phase contrast velocity imaging. The approach is directly extendable to three dimensions by systematically varying the first moment of gradient waveforms along each dimension and calculating the three velocity vector components (8–11). The time dimension can also be resolved using either prospective or retrospective cardiac gating. In the prospective approach data acquisition is synchronized to the cardiac cycle using a trigger signal generated from an ECG or plethysmograph (6). Other techniques acquire data in a continuous mode and retrospectively sort and interpolate the data using a simultaneously acquired cardiac signal (12, 13).

Although the phase contrast technique has proved to be a valuable tool for quantitative velocity imaging, its implementation using spin-warp acquisition strategies suffers from a number of problems. First, data inconsistencies between phase encode steps in ungated studies result in ghosting artifacts (14, 15) and degrade the accuracy of velocity measurements (16). Secondly, and more central to this article, acquisition times for time resolved (or *cine*) spin-warp based imaging are significant. This is

MRM 32:476–483 (1994)

From the McConnel Brain Imaging Center, Montreal Neurological Institute, McGill University, Montreal, QC, Canada (G.B.P.); Information Systems Lab, Department of Electrical Engineering, Stanford University, Stanford, California (C.H.M.); and Richard M. Lucas Center for MR Imaging and Spectroscopy, Department of Radiology, Stanford University, Stanford, California (T. J.B., N.J.P.).

Address correspondence to: Bruce Pike, Ph.D., Montreal Neurological Institute, WB-315, McGill University, 3801 University Street, Montreal, QC, Canada, H3A 2B4.

Received May 2, 1994; revised July 1, 1994; accepted July 5, 1994.

This work was supported by the Medical Research Council of Canada (GBP), Fonds de la Recherche en Santé du Québec (GBP), GE Medical Systems, National Institutes of Health (Grants RO1 HL39297, CA50948-(CHM), and HL46347(NJP)), and the Peter Allen fund.

0740-3194/94 $3.00

particularly limiting when attempting to resolve flow variations over the cardiac cycle in vessels of the abdomen and thorax. The respiratory motion in these regions makes it very desirable to image within one breath-hold. Depending on the desired temporal resolution, a conventional spin-warp phase contrast cine acquisition will take at least N_y heartbeats (N_y = number of phase encode steps). Clearly, for even a modest number of phase encodes (e.g., 128) the scan time is not within the limits of a single breath-hold. Solutions to this problem based upon "snap-shot" imaging strategies such as echo-planar (17, 18) and single shot spirals (19) have been demonstrated, but these techniques require specialized gradient systems and suffer from a variety of other limitations (20). K-space segmentation techniques (21, 22) allow a trade-off between high temporal resolution and total imaging time but cannot achieve both simultaneously.

In this article we present a general purpose phase contrast sequence based on a rapid interleaved spiral k-space trajectory acquisition (23). A major advantage of our technique is the ability to acquire time resolved velocity images along all three directions within a single breath hold using conventional imaging equipment. In addition, we show the method exhibits a marked reduction in pulsatility artifacts when used in an ungated mode. Experimental results from steady and pulsatile flow phantoms are also presented as are demonstrative results from healthy volunteers.

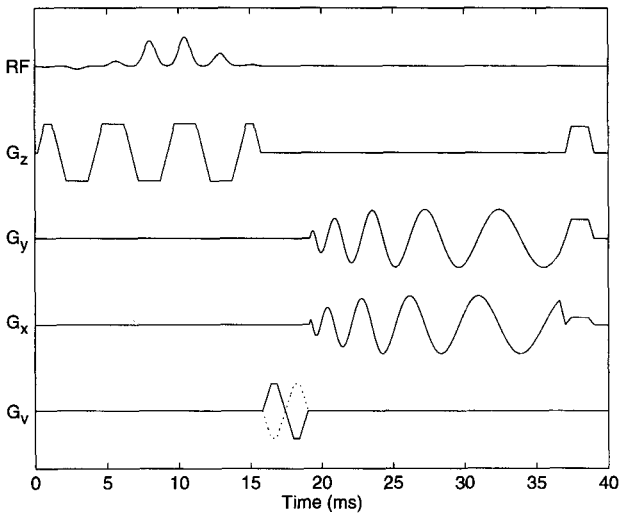

FIG. 1. Spiral phase contrast pulse sequence. Excitation is achieved using a spectral-spatial pulse and is immediately followed by bipolar flow encoding gradients. Although the flow encoding gradient is shown as a separate waveform here (G_v) it can be applied along any combination of logical axes and can be toggled on and off or inverted between measurements. The readout gradients trace a spiral trajectory in *k*-space and are followed by trapezoidal refocusing gradients. A constant amplitude spoiler gradient applied in the slice selection direction concludes the sequence.

METHODS

Pulse Sequence

A diagram of our phase contrast pulse sequence is shown in Fig. 1. The technique is a direct extension of the interleaved spiral imaging sequence described previously (23). Excitation is achieved via a 15.6 ms spectral-spatial pulse that selectively excites water protons within a Gaussian slice profile (24). The reasons for using a spectral-spatial pulse are twofold: improvement of the visualization of vessels surrounded by an otherwise high intensity fat signal, and avoidance of the blurring associated with off-resonance spins in spiral k-space trajectories. Although this pulse might appear relatively long, it is self-refocused (i.e. it requires no additional refocusing gradients) and has an effective center (point from which a maximal spin-echo would be generated) 6.2 ms before its end. The spectral-spatial pulse could of course be replaced with conventional fat saturation and slice selective pulses.

Bipolar flow-encoding gradients immediately follow excitation and are selectable in sensitivity (parameterized by *venc*, the velocity that produces a phase shift of π) and orientation. For single direction flow encoding the bipolar gradient can be toggled on and off between measurements (asymmetric flow encoding) or inverted (symmetric flow encoding). When all three flow directions are desired the operator can choose between a simple four point approach (11) (flow compensated, flow-encode *x*, flow-encode *y*, and flow-encode *z*) or a balanced technique that uses a Hadamard encoding strategy (9, 10). Time resolved imaging is achieved using prospective cardiac triggering. For these acquisitions, the differential flow-encodings may be interleaved within a single heartbeat or performed in sequential heartbeats. This permits an easy trade-off between temporal resolution and total imaging time.

The spiral readout gradients are selected based upon the desired field of view (FOV) and number of interleaves. Figure 1 illustrates 17.5 ms readout gradients that produce a theoretical in-plane resolution of 1.08 × 1.08 mm with 20 interleaves and a 200-mm FOV. These gradient waveforms have been numerically optimized to be slew rate limited (20 mT/m/ms) until they reach full-scale (10 mT/m) and are then amplitude limited. For the waveforms of Fig. 1 the first 4.8 ms of the readout gradient is slew-rate limited whereas the remaining 12.7 ms is amplitude limited. This *k*-space trajectory design approaches the goal of having constant linear velocity, which is optimal from an SNR standpoint because it improves the uniformity of the sampling density function that would ideally be flat, assuming no *a priori* knowledge of the image (25). At the end of each spiral, trapezoidal gradients are used to return to the origin of *k*-space (i.e. refocus) and a constant amplitude spoiler gradient is applied along the slice selection direction. Typically, 10 to 40 interleaves are acquired with each interleave being simply a rotated version of the basic waveform.

The pulse sequence shown in Fig. 1 has been implemented on a standard 1.5T imager (Signa; GE Medical Systems, Milwaukee, WI) with conventional gradients. The duration of each sequence repetition is approximately 35–40 ms depending upon the venc and readout gradient duration. This defines the maximum temporal

resolution achievable if flow encoding is not alternated within each heart beat. When multiple flow encodings are performed within a heartbeat the temporal resolution decreases by a factor of two (one direction) or four (three directions) as does the scan time.

Because off-resonance spins are blurred in spiral images, as opposed to shifted as in spin-warp images, each scan is preceded by the acquisition of a low spatial resolution field map. This is achieved using two single shot spirals with echo-shifted readouts. The calculated field map can be used in a variety of ways during reconstruction, the simplest of which is the selection of a single frequency for demodulation. This frequency can be chosen automatically as the mean or median value or can be user selected to correspond to a specific region of interest. If desired, multiple reconstructions can be performed retrospectively and combined to produce a globally deblurred image (26). For all the examples presented here a single frequency was used for demodulation.

Reconstruction

Following demodulation of the raw data for the selected resonance offset, a non-linear weighting is applied to each spiral interleaf to account for the non-uniform k-space sampling density. A gridding procedure is then used in which the data are convolved onto a two dimensional Cartesian matrix (27, 23) and Fourier transformed. The image amplitude modulation caused by the convolution is corrected by dividing the complex image by the Fourier transform of the gridding kernel. Velocity images are calculated using the difference in phase between complex images. More specifically, for complex images I_1 and I_2, acquired with first moments M_1 and M_2, the velocity image is calculated as:

$$v = \frac{arg[I_2 I_1^*]}{\gamma(M_2 - M_1)}, \quad [4]$$

where * denotes the complex conjugate and arg[I] is the phase of I. A magnitude image is also calculated as the average of magnitude images from each acquisition ($(|I_1| + |I_2|)/2$ in this example) and is multiplied by velocity to produce a magnitude-weighted velocity image. This image is useful for qualitative visualization of flow because it significantly suppresses the background noise present in the velocity image in regions of low signal magnitude (9). Complex difference processing can also be used, with the image being $|I_1 - I_2|$. This image provides a good visualization of the vascular anatomy and is useful in forming angiograms because it suppresses the signal from stationary tissue and does not exhibit high noise in regions of low signal intensity.

RESULTS

Phantom Experiments

A primary application of interest for spiral phase contrast imaging is flow quantitation in vessels of the abdomen and thorax. The usual protocol is to localize the vessel of interest and prescribe the phase contrast image orthogonal to the direction of flow. With this approach only one dimensional flow encoding in the slice selection direction is necessary. The volume flow rate is calculated from the resulting velocity image by defining the vessel boundary and multiplying the mean velocity by the vessel area.

To validate our technique for through plane flow quantitation we performed two sets of phantom experiments. The phantom consisted of a straight tube (12.7 mm inner diameter) passing through a stationary container filled with an agarose gel. For the first set of experiments, a solution of manganese chloride-doped water flowed through the tube fed by a gravity driven source that was maintained at a constant level using a pump. The flow rate was monitored throughout the experiment using an ultrasonic flowmeter (model T1010; Transonic Systems, Ithaca, NY) with an in-line probe placed 2 m from the isocenter. To avoid RF interference, the flowmeter was disabled during data readout using a blanking signal generated by the scanner (28). These measurements were also checked periodically using a graduated cylinder and stopwatch. Axial 2D spin-warp phase contrast ($TR/TE/\alpha$/venc = 50 ms/8 ms/30°/100 cm s^{-1}, 256 × 256 matrix, scan time 26 s) and spiral phase contrast ($TR/TE/\alpha$/venc = 50 ms/8.7 ms/30°/100 cm s^{-1}, 20 interleaves, scan time 2 s) images were acquired at a number of flow rates ranging from 0 to approximately 1200 ml/min. Flow rates were calculated from the phase contrast data using a semi-automated computer program that selects the vessel boundary using a percentage threshold (50%) on the magnitude image and applies the derived region-of-interest (ROI) to the corresponding velocity image. The results of this experiment are shown in Fig. 2 and indicate excellent agreement between the phase contrast and ultrasound measured flow rates (spin-warp phase contrast: slope = 1.027, R^2 = 0.999, standard error = 18.9 ml/min, spiral phase contrast: slope = 1.033, R^2 = 0.997, standard error = 11.9 ml/min).

To study pulsatile flow we conducted a second set of

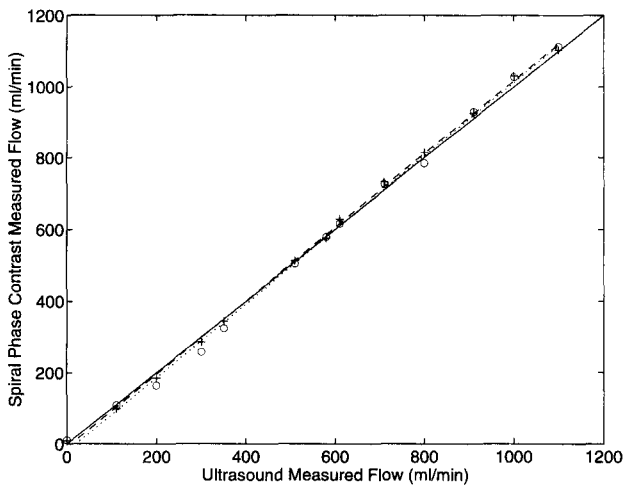

FIG. 2. Plot of spin-warp (+) and spiral (O) phase contrast measured flow rate versus ultrasound measured flow rate for a steady flow phantom. Excellent agreement is found for both the spin-warp (slope = 1.027, R^2 = 0.999, SE = 18.9 ml/min) and spiral (slope = 1.033, R^2 = 0.997, SE = 11.9 ml/min) techniques. The solid line is the line of identity, whereas the dashed and dotted lines are the spin-warp and spiral phase contrast regressions, respectively.

experiments in the same phantom using a pulsatile pump (Pulsatile Blood Pump, model 1421; Harvard Apparatus, South Natick, MA). A plethysmograph sensor on the pump outlet produced a reliable gating signal. The ultrasound flowmeter signal was sampled and stored every 20 ms using a personal computer (Macintosh IIci; Apple Computer, Cupertino, CA), equipped with data acquisition hardware and software (Workbench; Strawberry Tree, Sunnyvale CA). The blanking and trigger signals were also digitized and stored. A composite ultrasound flow waveform was calculated by binning and averaging all valid (nonblanked) flow samples in each of the intervals in the cycle. The pulsatile pump was adjusted to have a period of approximately 1 s and two experiments were performed with average flow rates of approximately 350 ml/min and 500 ml/min. In each case gated spiral phase contrast acquisitions were performed with *TR/TE/α*/venc = 41 ms/8.7 ms/30°/100 cm s^{-1}, 20 interleaves, and flow encoding in the slice select direction. A total of 23 measurements (time frames) were acquired per pump cycle with flow encoding in alternate cycles, thus bringing the total scan time to approximately 40 s. Flow values were calculated from the phase contrast images using the technique described above, with a separate region of interest defined in each time frame. Figures 3a and 3b are plots of the ultrasound and spiral phase contrast measured flow waveforms for the 350 ml/min and 500 ml/min experiments, respectively. A scatter plot of all the spiral phase contrast data points versus the corresponding ultrasound data from the pulsatile flow experiments is shown in Fig. 3c. Linear regression of these data gave: slope = 1.036, R^2 = 0.968, and a standard error of 49.4 ml/min.

In Vivo Experiments

We have qualitatively evaluated the performance of the spiral phase contrast sequence in a number of normal volunteers. A comparative example of ungated spin-warp and spiral acquisitions of the carotid arteries is shown in Fig. 4. Scan parameters common to both sequences were: *TR/TE/α*/venc = 50 ms/8.7 ms/45°/100 cm s^{-1}. The spin-warp data were acquired on a 256 × 256 matrix, whereas the spiral data were acquired with 20 interleaves, thus giving scan times of 26 and 2 s, respectively and an SNR difference of approximately 2:1 (spin-warp : spiral). As expected, the spin-warp images exhibit the familiar ghosting artifacts in the phase encoding direction (anterior-posterior) due to view-to-view phase and magnitude inconsistencies. The same inconsistencies probably occur in the spiral acquisition but result in a "swirling" artifact that empirically appears less troublesome. This is likely due to both the spiral trajectory itself and the redundant sampling at low spatial frequencies. These effects are particularly apparent in the magnitude-weighted velocity images that show significant carotid artery ghosting in the spin-warp data but no gross artifacts in the spiral image. Note that in these magnitude-weighted velocity images bright regions represent flow in the superior-inferior direction, dark represent inferior-superior flow, and mid-grey represent stationary tissue.

In gated studies, the reduced scan time of the spiral sequence (~20–40 heartbeats) permits high temporal resolution breath-held acquisitions free of respiratory artifacts. Because conventional spin-warp measurements with comparable resolution cannot be acquired in a breath-hold, comparative studies were not performed.

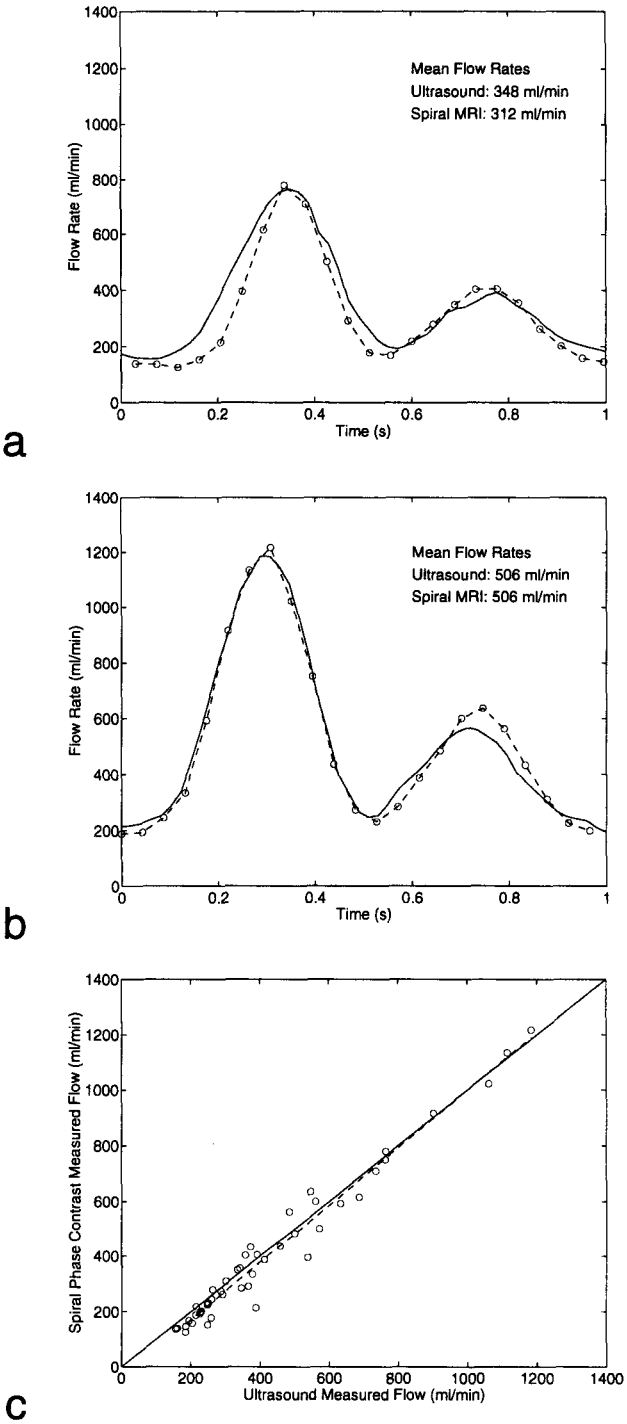

FIG. 3. Pulsatile flow phantom results. The ultrasound (solid line) and spiral phase contrast ('o' and dashed line) measured flow waveforms are plotted for two average flow rates (a and b). (c) shows a plot of all the MRI versus ultrasound flow data. The solid line is the line of identity and the regression is shown as a dashed line (slope = 1.036, R^2 = 0.968, SE = 49.4 ml/min).

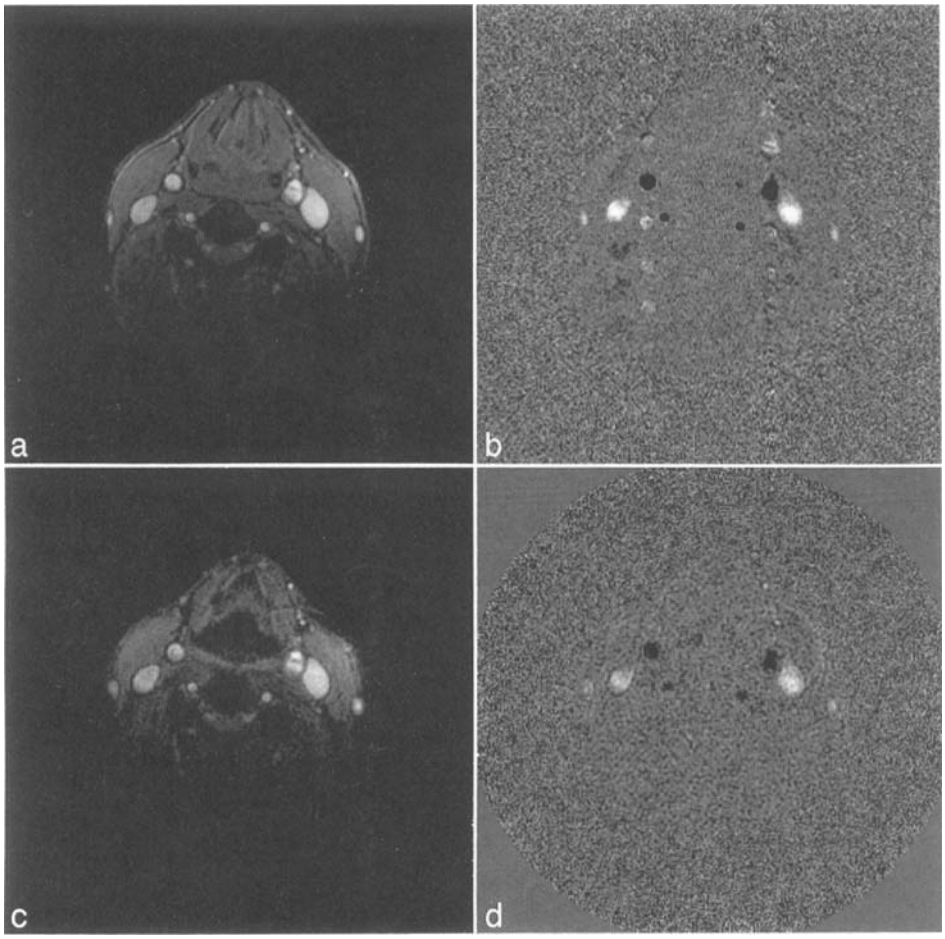

FIG. 4. Spin-warp magnitude (a) and magnitude-weighted velocity (b) images and corresponding spiral images (c and d) of the neck of a normal volunteer. In the magnitude weighted velocity images flow in the superior-inferior direction (venous) is shown as a bright signal, inferior-superior flow (arterial) is shown as a dark signal, and mid-gray values represent stationary tissue. Note the ghosting artifacts emanating from the carotid arteries in (b) and the lack thereof in (d).

An example of a cardiac gated study of the renal artery and vein is shown in Fig. 5. These data were acquired using a flexible surface coil wrapped around the left side of the abdomen of a volunteer. Shown in Fig. 5a and b are the magnitude and magnitude-weighted velocity images that represent one time frame (early systole) of this doubly oblique, 18 cardiac frame, single axis (through plane), 20 interleaf spiral measurement. The slice thickness was 5 mm, $TR/TE/\alpha$/venc were 41 ms/8.7 ms/30°/100 cm s^{-1}, and noninterleaved flow encoding was used. All data were acquired in a single 40-heartbeat breath-hold that translated to approximately 30 s for this individual (heart rate ~75 BPM). The slice was oriented to be orthogonal to the renal artery (arrowhead) but also well visualized are the renal vein (small arrow) and the descending aorta (large arrow). With the flow analysis program described above, these vessels were contoured on each magnitude image and the resulting ROIs applied to the velocity images for calculation of flow. The calculated mean flow rates were 312, 352, and 890 ml/min for the renal artery, renal vein, and descending aorta respectively. Fig. 5c shows the flow waveform for the aorta. Although these measurements could not be verified using another technique, the mean flow rates and flow waveforms were as expected for a normal individual. The arterial and venous renal flow rates were also in good agreement with each other considering the contribution to left renal vein flow due to the gonadal vein.

A third *in vivo* demonstration of our technique is presented in Fig. 6. In this example a normal volunteer was imaged in the prone position using a 127-mm (5-inch) surface coil. A double oblique slice was then used with ECG triggering to obtain a short axis view of the heart at 24 time points in the cardiac cycle. Noninterleaved flow encoding was performed along all three directions with 10 spiral interleaves (1.56 × 1.56 mm resolution) thereby giving a 40-heartbeat acquisition time (~40 s) that was within one breath-hold for this individual. Other scan parameters were as described above for the renal study with the exception of venc that was 75 cm s^{-1}. Fig. 6a shows a magnitude image from early systole whereas corresponding right-left, anterior-posterior, and superior-inferior magnitude-weighted velocity images are shown in Fig. 6b–6d, respectively.

DISCUSSION

The primary quantitative application of the technique considered in this article is through plane flow quantitation; therefore, our phantom experiments have been limited to this configuration. For the steady flow phantom experiments, agreement between ultrasound and MRI phase contrast measured flow was excellent over a large range of flows. The time resolved pulsatile flow phantom results showed a greater variation between ultrasound and MRI but are nonetheless in very good agreement.

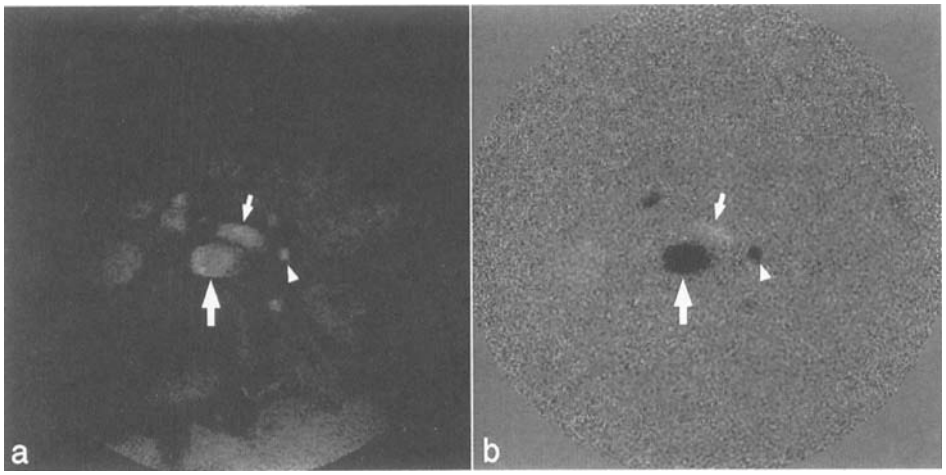

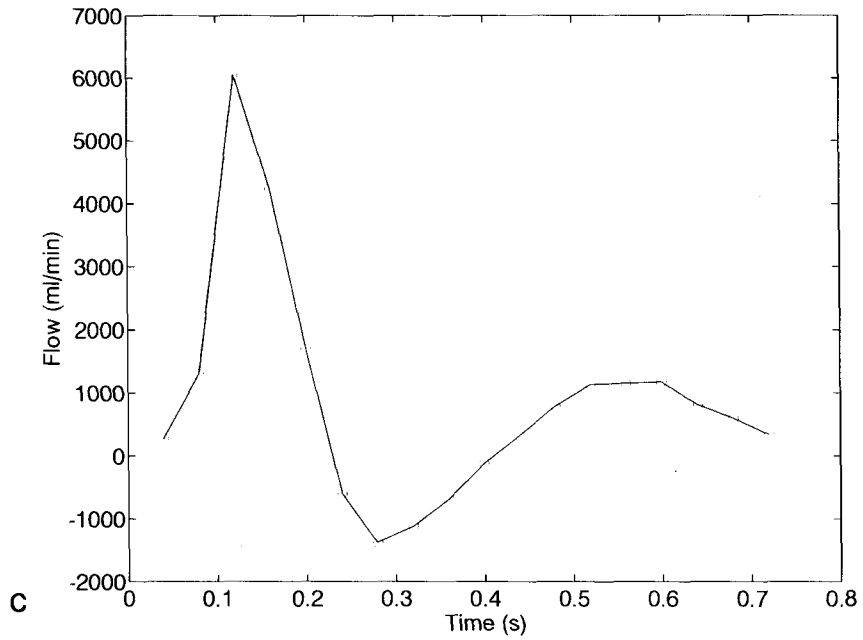

FIG. 5. Spiral phase contrast magnitude (a) and magnitude-weighted through plane velocity (b) images of the left renal artery (arrowhead), renal vein (small arrow), and descending abdominal aorta (large arrow) of a normal volunteer. These images represent one time frame (early systole) from an 18-phase cardiac gated breath-held acquisition. (c) shows the measured flow waveform in the aorta (mean flow = 890 ml/min).

Furthermore, the mean flow calculated from each of the spiral MRI images was within the ±10% error figure quoted for the ultrasound flow meter. The *in vivo* renal study, although not a quantitative validation of our method, produced self consistent results that were within the expected range for a normal individual.

In-plave velocity quantitation has not been validated in this study. However, there are at least two reasons to believe spiral scanning is well suited to this application (23). First is the fact that spiral trajectories start at the origin and move outwards. Therefore, with the exception of the effects of the bipolar flow encoding gradient, the spiral readouts collect the center of *k*-space with zero moments of all orders. Second is that all moments of the readout gradients periodically return to zero together.

For ungated angiography the spiral sequence showed some swirling artifacts as opposed to the familiar ghosting that occurs in spin-warp acquisitions. The result is esthetically less bothersome (see Fig. 4) because in spin-warp images the effect is focused into ghosts that might mimic vessels whereas the swirling pattern in the spiral images is more diffuse and cannot be mistaken for such. There may also be an advantage in quantitative ungated flow measurements using the spiral technique because the swirling artifacts emanating from a vessel are not likely to fall back upon that vessel. This is not the case for spin-warp based acquisitions and can represent a significant source of error (29). This point requires further investigation.

The main advantages of the interleaved spiral approach to phase-contrast velocity imaging are the short acquisition times and the applicability to conventional imaging systems. In particular, the fact that single slice time-resolved velocity images can be acquired within a single breath-hold represents a significant improvement over conventional spin-warp techniques. In the examples presented here normal volunteers were imaged using 40 heartbeat breath-holds (~30–40 s) that may be too long for patients. However, two approaches to reducing this time are immediately available: reduce the spatial resolution, and/or reduce the temporal resolution. An example of the first approach was illustrated in Fig. 6 in

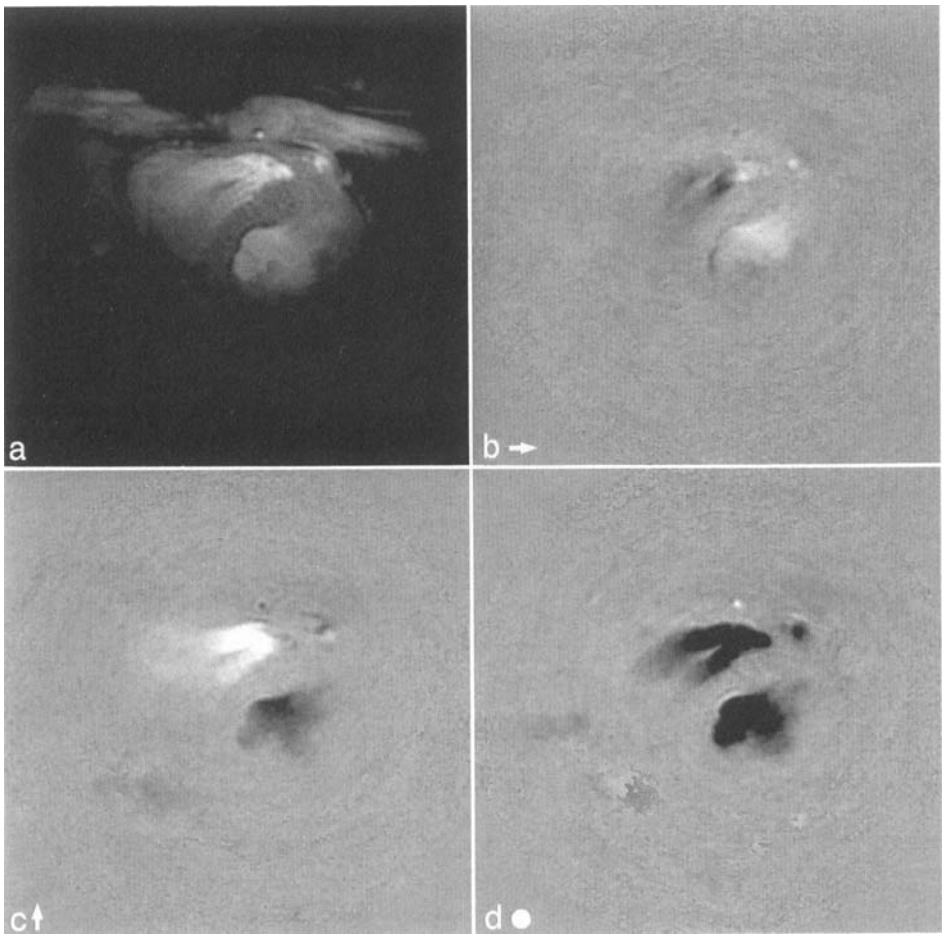

FIG. 6. One time frame of a 24-phase cardiac-gated spiral phase contrast acquisition of the short axis of the heart. Shown are the magnitude (a) and magnitude-weighted velocity images for right-left (b), anterior-posterior (c), and superior-inferior (d) flow directions, respectively.

which the number of interleaves was reduced to 10, thus compromising the spatial resolution to acquire velocity images in all three directions within 40 heartbeats. This approach is of course also applicable to single axis velocity encoding and would result in a scan time of only 20 heartbeats (~15–20 s). Reducing the temporal resolution is easily achieved by interleaving two or more flow encodings within each heartbeat. In our implementation the sequence time, and hence maximum temporal resolution, is ~40 ms. Therefore, interleaving two flow encodings should still produce acceptable temporal resolution for many applications. Both approaches to scan time reduction can also be employed simultaneously. For example, a complete three direction time-resolved data set could be acquired within a 20 heartbeat breath-hold using 10 spiral interleaves and 2 flow measurement interleaving.

Although reducing spatial and/or temporal resolutions represents simple approaches to decreasing scan time a more desirable solution is to improve imaging hardware. Specifically, increasing the maximum gradient strength and slew rates would allow acquisition of the same amount of data in fewer interleaves. The imager used in our experiments had a maximum gradient strength of 10 mT/m with a rise time of 600 μs. Although these specifications are typical of current gradient systems, the next generation of equipment will likely show significant improvements. Assuming, for example, our maximum gradient strength and slew rate were doubled, we note that the number of interleaves could be reduced by approximately 30–40% without compromising resolution. Of more importance than specific numbers however, is the fact that interleaved spiral k-space trajectories constitute an efficient fast imaging technique that is well suited to phase-contrast imaging. The inherent efficiency of a spiral trajectory holds for any non-resonant gradient system. This is demonstrated by the fact that a well designed spiral gradient waveform will always be either slew rate or maximum amplitude limited thus ensuring the most efficient use of gradient hardware.

In addition to through plane flow quantitation a variety of other applications of our spiral technique exist. For example, using the same acquisition parameters as those of Fig. 6, but decreasing the venc to 15–20 cm s^{-1}, we have obtained images of myocardial velocities. These data can be analyzed to determine the translation, rotation, and deformation of retrospectively selected regions of the myocardium throughout the cardiac cycle (30). Another obvious application, given the sequence's robustness in the presence of pulsatile flow, is the rapid acquisition of phase contrast angiograms. Three dimensional (3D) angiograms could be acquired by adding a phase encoding gradient in the slice select direction or by using some form of a 3D spiral. A related, but more ambitious, application would be to acquire the complete 3D,

time resolved, velocity vector data set for a vessel segment of interest and to retrospectively calculate particle streamlines (31) or pressure distribution (32).

In conclusion, we have developed a rapid phase contrast imaging sequence based on interleaved spiral k-space acquisitions. The technique has been validated on steady and pulsatile flow phantoms and tested in normal volunteers. The ability to acquire high resolution cardiac gated velocity images within a single breath-hold provides exciting possibilities for this method.

ACKNOWLEDGMENTS

The authors thank Bob Hu, Graham Sommer, and Herbert Wegmueller for their assistance in imaging volunteers.

REFERENCES

1. E. L. Hahn, Detection of sea-water motion by nuclear precession. *J. Geophys. Res.* **65(2),** 776–777 (1960).
2. P. R. Moran, A flow velocity zeugmatographic interlace for NMR imaging in humans. *Magn. Reson. Imaging* **1,** 197–203 (1982).
3. P. V. Dijk, Direct cardiac NMR imaging of heart wall and blood flow velocity. *J. Comput. Assist. Tomogr.* **8(3),** 429–436 (1984).
4. M. O'Donnell, NMR blood flow imaging using multiecho, phase contrast sequences. *Med. Phys.* **12(1),** 59–64 (1985).
5. C. L. Dumoulin, H. R. Hart, Magnetic resonance angiography. *Radiology* **161,** 717–720 (1986).
6. G. L. Nayler, D. N. Firmin, D. B. Longmore, Blood flow imaging by cine magnetic resonance. *J. Comput. Assist. Tomogr.* **10,(5)** 715–722 (1986).
7. L. Axel and D. Morton, MR flow imaging by velocity compensated/uncompensated difference images. *J. Comput. Assist. Tomogr.* **11,(1)** 31–34 (1987).
8. C. L. Dumoulin, S. P. Souza, M. F. Walker, and W. Wagle, Three-dimensional phase contrast angiography. *Magn. Reson. Med.* **9,** 139–149 (1989).
9. N. J. Pelc, M. A. Bernstein, A. Shimakawa, and G. H. Glover, Encoding strategies for three-direction phase-contrast MR imaging of flow. *J. Magn. Reson. Imaging.* **1,** 405–413 (1991).
10. C. A. Dumoulin, S. P. Souza, D. D. Darrow, N. J. Pelc, J. W. Adams, S. A. Ash, Simultaneous acquisition of phase-contrast angiograms and stationary-tissue images with hadamard encoding of flow-induced phase shift. *J. Magn. Reson. Imaging.* **1,** 399–404 (1991).
11. R. Hausmann, J. S. Lewin, G. Laub, Phase-contrast MR angiography with reduced acquisition time: New concepts in sequence design. *J. Magn. Reson. Imaging.* **1,** 415–422 (1991).
12. G. H. Glover, A rapid-gated cine MRI technique. *in* "Magnetic Resonance Annual," pp. 299–333, Raven, New York, 1988.
13. N. J. Pelc, R. J. Herfkens, A. Shimakawa, and D. R. Enzmann, Phase contrast cine magnetic resonance imaging. *Magn. Reson. Q.* **7(4),** 229–254 (1991).
14. M. L. Wood, R. M. Henkelman, MR image artifacts from periodic motion. *Med. Phys.* **12(2),** 143–151 (1985).
15. W. H. Perman, P. R. Moran, R. A. Moran, M. A. Bernstein, Artifacts from pulsatile flow in MR imaging. *J. Comput. Assist. Tomogr.* **10,** 473–483 (1986).
16. N. J. Hangiandreou, P. J. Rossman, S. J. Rieder, Analysis of MR phase-contrast measurements of pulsatile velocity waveforms. *J. Magn. Reson. Imaging.* **3,** 387–394 (1993).
17. D. N. Firmin, R. H. Klipstein, G. L. Hounsfield, M. P. Paley, D. B. Longmore, Echo-planar high-resolution flow velocity mapping. *Magn. Reson. Med.* **12,** 316–327 (1989).
18. D. N. Guilfoyle, P. Gibbs, R. J. Ordidge, P. Mansfield, Real-time flow measurements using echo-planar imaging. *Magn. Reson. Med.* **18,** 1–8 (1991).
19. P. D. Gatehouse, D. N. Firmin, R. L. Hughes, S. Collins, D. B. Longmore. Phase contrast velocity mapping by spiral scanning, *in* "Proc. SMRM, 11th Annual Meeting, Berlin, Germany 1992, p. 216."
20. D. N. Firmin, P. D. Gatehouse, D. B. Longmore, Comparison of snap-shot quantitation flow imaging techniques, *in* "Proc. SMRM, 11th Annual Meeting, Berlin, Germany 1992," p. 2915.
21. D. J. Atkinson, R. R. Edelman, Cineangiography of the heart in a single breath hold with a segmented turboflash sequence. *Radiology.* **178,** 357–360 (1991).
22. J. O. Fredrickson, N. J. Pelc, Time-resolved MR imaging by automatic data segmentation. *J. Magn. Reson. Imaging.* **4(2),** 189–196 (1994).
23. C. H. Meyer, B. S. Hu, D. G. Nishimura, A. Macovski, Fast spiral coronary artery imaging. *Magn. Reson. Med.* **28,** 202–213 (1992).
24. C. H. Meyer, J. M. Pauly, A. Macovski, D. G. Nishimura, Simultaneous spatial and spectral selective excitation. *Magn. Reson. Med.* **15,** 287–304 (1990).
25. A. Macovski and C. H. Meyer, A novel fast-scanning system. *in* "Proc. SMRM, 8th Annual Meeting, Montreal, Canada, 1986," p. 156.
26. D. C. Noll, C. H. Meyer, J. M. Pauly, D. G. Nishimura, A. Macovski, A homogeneity correction method for magnetic resonance imaging with time-varying gradients, *IEEE. Trans. Med. Imaging.* **10(4),** 629–637 (1991).
27. J. I. Jackson, C. H. Meyer, D. G. Nishimura, A. Macovski, Selection of a convolution function for Fourier inversion using gridding. *IEEE. Trans. Med. Imaging.* **10(3),** 473–478 (1991).
28. L. R. Pelc, N. J. Pelc, S. C. Rayhill, L. J. Castro, G. H. Glover, Arterial and venous blood flow: noninvasive quantitation with mr imaging. *Radiology.* **185(3),** 809–812 (1992).
29. R. L. Wolf, R. L. Ehman, S. J. Riederer, P. J. Rossman, Analysis of systematic and random error in MR volumetric flow measurements. *Magn. Reson. Med.* **30,** 82–91 (1993).
30. N. J. Pelc, R. J. Herfkens, L. R. Pelc, 3D analysis of myocardial motion and deformation with phase contrast cine MRI, *in* "Proc. SMRM, 11th Annual Meeting, Berlin, Germany, 1992," p. 18.
31. S. Napel, D. H. Lee, R. Frayne, B. K. Rutt, Visualizing three-dimensional flow with simulated streamlines and three-dimensional phase-contrast MR imaging. *J. Magn. Reson. Imaging.* **2,** 143–53 (1992).
32. S. M. Song, B. S. Hu, S. Napel, N. J. Pelc, G. H. Glover, Obtaining spatial pressure distributions from phase-contrast velocity data, *in* "Proc. RSNA, 79th Annual Meeting, Chicago, 1993," p. 270.